

Multivariable Model-less Feedforward Control of a Monolithic Nanopositioning Stage With FIR Filter Inversion

Meysam Omidbeike¹, Arnfinn A. Eielsen², Yuen K. Yong¹, Andrew J. Fleming¹

Abstract—A model-less approach for inversion of the dynamics of multivariable systems using FIR filters is described. Inversion-based feedforward techniques have been widely used in the literature to achieve high-performance output tracking. The foremost difficulties associated with plant inversions are model uncertainties and non-minimum phase zeros. Various model-based methods have been proposed to exclude non-minimum phase zeros when inverting both single-input and single-output (SISO), and multiple-input and multiple-output (MIMO) systems. However, these methods increase the model uncertainty as they are no longer exact. To overcome these difficulties a model-less approach using FIR filters is presented. The results when applying the feedforward FIR filter to a multivariable nanopositioning system is presented, and they demonstrate the effectiveness of the feedforward technique in reducing the cross-coupling and achieving significantly improved output tracking.

I. INTRODUCTION

Nanopositioners are electro-mechanical devices capable of generating high-resolution motion in up to six degrees of freedom (DOF) [1]. Common nanopositioning applications include scanning probe microscopy, lithography and hard disk drives [2]–[5]. In this paper, a new monolithic nanopositioner is introduced [6]. Parallel actuators driving a central platform are etched into a bi-morph piezoelectric sheet to provide both actuation and guidance of the moving platform [7,8]. The actuator configuration for this stage yields five DOF. The stage, mounted on an insulating base, is shown in Fig. 1. Details on the design and manufacturing and process can be found in [6,9].

Inversion of system dynamics can be used to achieve high tracking performance [2]–[5]. Compared to feedback control, which reacts to the measured tracking error, a feed-forward controller uses the inverse of a model to generate a control signal [5]. The model can include effects such as the plant dynamics, creep and hysteresis [2]. If the model is invertible and sufficiently accurate, the feed-forward control signal will improve tracking performance [10]. The foremost difficulties associated with inversion are non-minimum phase zeros (NMP) [11] and model uncertainties [10].

Feed-forward control has been widely studied in the literature and various methods for NMP systems have been proposed. A model-based method for single-input and single-output (SISO) systems is the zero-phase error tracking con-



Fig. 1. Monolithic bi-morph nanopositioner mounted on a base.

troller (ZPETC) [12]. Here, the minimum phase, or stable, zeros of an infinite impulse response (IIR) model of the plant are inverted while the conjugate of the NMP zeros are used to cancel the phase of the plant. The effectiveness of the inversion is highly dependent on the accuracy of an identified IIR model, and the accuracy in terms of the amplitude response is deteriorated due to the NMP zeros. This method cannot be extended to multiple-input and multiple-output (MIMO) systems but other inversion methods are applicable [13]–[15]. In [15], plant inversion is found to improve tracking for a piezoelectric tube-actuator. This method is effective in applications with a known, sufficiently smooth reference. In applications with an unknown reference, preview-based stable inversion approaches can be used [13,14]. However, the successful implementation of these methods is dependent on the accuracy of the identified model.

An alternative to model-based inversion methods is a finite impulse response (FIR) filter inverse [16,17]. An FIR inverse overcomes the difficulties associated with NMP zeros and system identification. This paper presents a method for producing a MIMO FIR inverse. The empirical transfer function estimate (ETF) matrix for the MIMO system is computed by independently measuring the response of each input-output pair. The inverse responses are found numerically from the ETF matrix, and the FIR filter coefficients that best fit to the inverse responses are found using least-squares optimisation. To keep the FIR filter length reasonable, the impulse response is truncated, and some distortion of the frequency response occurs. However, this is counteracted by using a suitable window function. The results is a highly accurate MIMO FIR filter inverse which can be used for feed-forward control, as well as repetitive control (RC) and iterative learning control (ILC).

¹M. Omidbeike, A. J. Fleming and Y. K. Yong are with the Precision Mechatronics Lab, Faculty of Engineering and Built Environment, The University of Newcastle, Callaghan 2308, New South Wales, Australia {meysam.omidbeike, yuenkuan.yong, andrew.fleming}@newcastle.edu.au.net

²A. A. Eielsen is with the Faculty of Science and Technology, Department of Electrical Engineering and Computer Science, University of Stavanger, Norway arnfinn.a.eielsen@uis.no

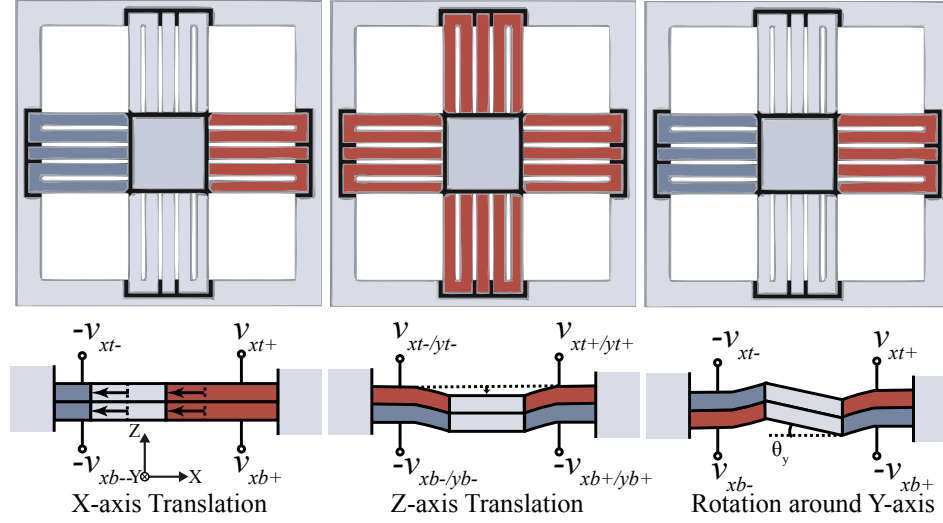


Fig. 2. Applied voltages generating motion in five degrees of freedom (DOF).

II. MONOLITHIC NANOPositionER

The design and manufacturing process of the nanopositioning stage used in this work is the same as the monolithic stage described in [6] but here a bi-morph piezoelectric sheet is used in order to increase the DOF from two to five. The sheet is cut to create parallel actuators that move a central platform. The nanopositioning stage mounted on an insulating base is shown in Fig. 1. An analysis of the stage is published alongside this paper [9].

The applied voltages generating motion are shown in Fig. 2. Assuming that each layer is outwardly poled, with the middle layer grounded, a positive voltage applied to the top and bottom electrodes will cause the beam to expand and displace the central platform away from the positive voltage. For example, when a positive voltage is applied to v_{xt+} and v_{xb+} , and an equal and opposite voltage is applied to v_{xt-} and v_{xb-} , the central platform will translate in the negative X -direction.

The stage has 8 inputs and 5 outputs, where the inputs are the applied voltages to the top and bottom electrodes and the outputs are the translations along the X -, Y - and Z -axes and the rotations around the X - and Y -axes. The electrode voltages can be grouped in order to correspond to the three translations and two rotations. This is done by creating a transformation matrix that maps the five inputs that relate to the translations and rotations to the eight specific electrode voltages. Using this transformation, the system is square with five inputs and five outputs. The inputs are $u_x, u_y, u_z, u_{\theta_x}$ and u_{θ_y} and the outputs are the translations d_x, d_y and d_z and rotations θ_x and θ_y .

A. Transformation Matrix (Jacobian)

The transformation matrix is denoted \mathbf{J} , and maps the five inputs

$$\mathbf{u} = [u_x \ u_y \ u_z \ u_{\theta_x} \ u_{\theta_y}]^T$$

to the eight physical electrode voltages

$$\mathbf{v} = [v_{xt+} \ v_{xb+} \ v_{xt-} \ v_{xb-} \ v_{yt+} \ v_{yb+} \ v_{yt-} \ v_{yb-}]^T$$

using the expression $\mathbf{v} = \mathbf{J}\mathbf{u}$. The transformation matrix \mathbf{J} encodes how the inputs \mathbf{u} generates motion via the electrode voltages \mathbf{v} . For example, the first column of \mathbf{J} corresponds to translation along the X -axis where the top and bottom actuators on each side are driven with equal and opposite voltages. Therefore, electrodes for the motion in the X -axis are selected by using elements ± 1 , where the sign is determined by the needed polarity of the applied voltage. Similarly, selecting the electrodes using elements ± 1 according to which motions are desired, the transformation from \mathbf{u} to \mathbf{v} can be constructed as

$$\begin{bmatrix} v_{xt+} \\ v_{xb+} \\ v_{xt-} \\ v_{xb-} \\ v_{yt+} \\ v_{yb+} \\ v_{yt-} \\ v_{yb-} \end{bmatrix} = \begin{bmatrix} 1 & 0 & 1 & 0 & 1 \\ 1 & 0 & -1 & 0 & -1 \\ -1 & 0 & 1 & 0 & -1 \\ -1 & 0 & -1 & 0 & 1 \\ 0 & 1 & 1 & 1 & 0 \\ 0 & 1 & -1 & -1 & 0 \\ 0 & -1 & 1 & -1 & 0 \\ 0 & -1 & -1 & 1 & 1 \end{bmatrix} \begin{bmatrix} u_x \\ u_y \\ u_z \\ u_{\theta_x} \\ u_{\theta_y} \end{bmatrix}. \quad (1)$$

The naming convention used for the electrode voltages \mathbf{v} is according to Fig. 2, where the subscript denotes the direction and layer. The product $\mathbf{J}\mathbf{u}$ can be found as

$$\begin{bmatrix} v_{xt+} \\ v_{xb+} \\ v_{xt-} \\ v_{xb-} \\ v_{yt+} \\ v_{yb+} \\ v_{yt-} \\ v_{yb-} \end{bmatrix} = \begin{bmatrix} u_x + u_z + u_{\theta_y} \\ u_x - u_z - u_{\theta_y} \\ -u_x + u_z - u_{\theta_y} \\ -u_x - u_z + u_{\theta_y} \\ u_y + u_z + u_{\theta_x} \\ u_y - u_z - u_{\theta_x} \\ u_y + u_z - u_{\theta_x} \\ u_y - u_z + u_{\theta_x} \end{bmatrix}. \quad (2)$$

Considering (1), it can be seen that \mathbf{J} is the Jacobian matrix of the right hand side of (2).

III. EXPERIMENTAL SET-UP

For this work, the nanopositioner was used as a vertical stage with translation along the Z -axis, and rotations around the X - and Y -axes. The experimental configuration is shown

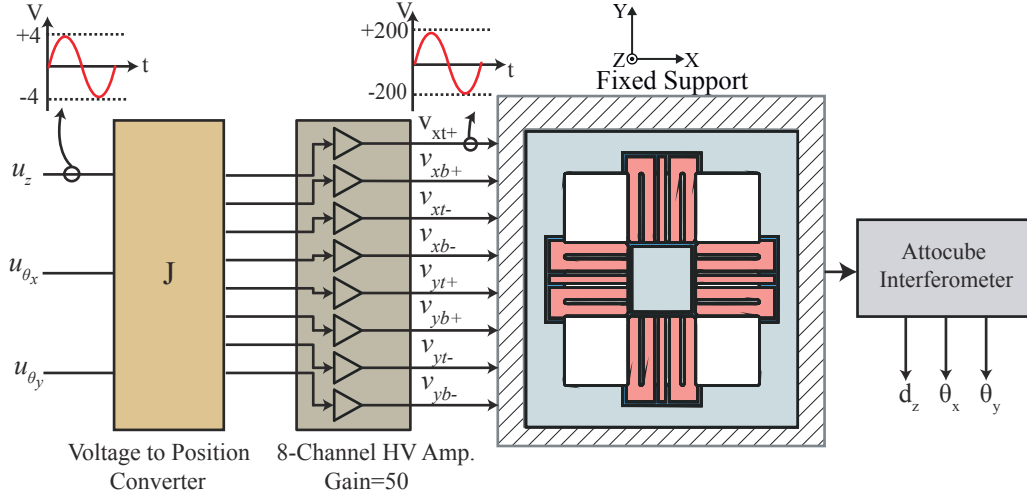


Fig. 3. Experimental configuration of the monolithic nanopositioner.

in Fig. 3. The translation and rotations, d_z , θ_x and θ_y , were measured by an Attocube FPS3010 laser interferometer. A custom circuit implementing the Jacobian matrix \mathbf{J} was used to produce the eight electrode voltages. The stage was driven by an eight-channel high-voltage amplifier, where each channel has a gain of 50. The control law was implemented using a dSPACE DS1103 hardware-in-the-loop system via Simulink Coder.

The full operating range of the nanopositioner is from -200 V to $+500$ V. However, for safety reasons, a range of -200 V to $+200$ V was chosen, resulting in a total range of $26.5 \mu\text{m}$ along the Z -axis, 600 mdeg rotation around the X -axis and 884 mdeg rotation around Y -axis. The open-loop frequency responses, with 4001 frequency samples, for each input-output pair of the 3×3 system are shown in Fig. 4. They were obtained by the method described in Sec. IV. The sampling frequency used was 20 kHz and the FIR filters were designed with $N = 400$ taps.

IV. DESIGN OF MIMO MODEL-LESS FIR FILTER

An alternative to model-based control design is to use model-less, or empirical, FIR filters. This eliminates the need for model-based multivariable system identification. This is important because system identification methods frequently fail in terms of finding accurate models of a reasonable order, and can yield models that are ill-conditioned for numerical computations, that are unstable and have NMP zeros. FIR filters also overcome the difficulties associated with inversion of NMP zeros.

The model-less FIR filter method is based on non-parametric frequency-domain system identification, which is used to generate an empirical transfer-function estimate (ETF) matrix. The FIR filters are then synthesised directly using the measured frequency response. The accuracy of a FIR filter is mainly determined by the number of taps [16].

Consider a MIMO plant model with m inputs and l outputs described by

$$\mathbf{Y}(k) = \hat{\mathbf{G}}(k)\mathbf{U}(k) \quad (3)$$

where

$$\mathbf{U}(k) = [U_1(k), U_2(k), \dots, U_m(k)]^T,$$

denotes the input vector and

$$\mathbf{Y}(k) = [Y_1(k), Y_2(k), \dots, Y_m(k)]^T$$

denotes the output vector, and $\hat{\mathbf{G}}(k)$ is an $l \times m$ ETFE matrix. The ETFE $\hat{G}_{ij}(k)$, relating the j^{th} input to the i^{th} output of $\hat{\mathbf{G}}(k)$, is given by [18]

$$\hat{G}_{ij}(k) = \frac{Y_j(k)}{U_i(k)}, \quad (4)$$

where $U_i(k)$ and $Y_j(k)$ are the discrete Fourier transforms (DFT) of the input and output

$$Y_j(k) = \sum_{n=0}^{M-1} y_j(n) e^{-j2\pi kn/M}, \quad (5)$$

and

$$U_i(k) = \sum_{n=0}^{M-1} u_i(n) e^{-j2\pi kn/M}, \quad (6)$$

with $k = 0, 1, \dots, M-1$. This estimate is empirical as no other assumptions have been imposed other than linearity. Exciting one input at a time with white Gaussian noise and recording the input and output data, each element in $\hat{\mathbf{G}}(k)$ can be estimated using (4) [16,17]. To obtain a more accurate ETFE, sectioning and time averaging of the recorded data can be used [19].

The inverse response of the MIMO system can be found by inverting the ETFE matrix $\hat{\mathbf{G}}(k)$ obtained from (4), by numerically solving for $\hat{\mathbf{G}}^{-1}(k)$ in the equation

$$\hat{\mathbf{G}}(k)\hat{\mathbf{G}}^{-1}(k) = \mathbf{I}_n, \quad (7)$$

where \mathbf{I}_n denotes the identity matrix and n is the dimension of the ETFE matrix $\hat{\mathbf{G}}(k)$. The elements of $\hat{\mathbf{G}}^{-1}(k)$ are henceforth denoted $H_{ij}(k)$. There will be a unique solution if the transfer function matrix $\hat{\mathbf{G}}(k)$ if $l = m$, i.e. if it is square.

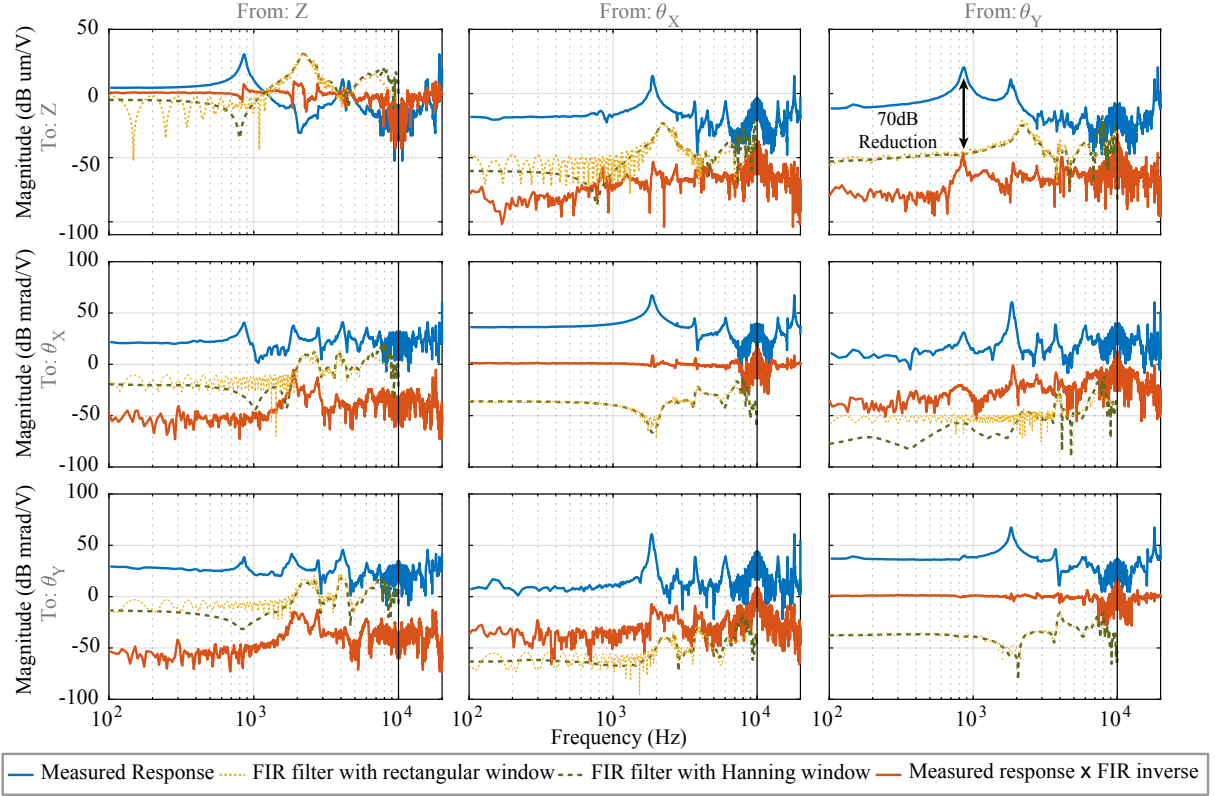


Fig. 4. Frequency responses for all input-output pairs: measured responses, FIR filter inverses with and without windowing, and the product between the measured responses and the FIR filter inverses. Note that for the product, the diagonal elements are approximately unity, and the off-diagonal elements are greatly reduced, compared to the original measured response, indicating that cross-coupling has been reduced significantly.

The inverse plant response as an FIR filter can be found by using least-squares optimisation. This is advantageous, as the filter length, or number of taps, can be different than the number of frequency samples in the measured response. Using the frequency samples directly would amount to using the frequency-sampling method for FIR filter synthesis [20].

An FIR filter transfer-function is given as

$$F_{ij}(z^{-1}) = z^q(a_0 + a_1 z^{-1} + \dots + a_{p-1} z^{-p+1}) = z^q \mathbf{a}^T \mathbf{z}, \quad (8)$$

where $p, q \in \mathbb{N}_0$,

$$\mathbf{a} = [a_0, a_1, \dots, a_{p-1}]^T, \text{ and } \mathbf{z} = [1, z^{-1}, \dots, z^{-p+1}]^T.$$

A desired filter length p must be chosen, and q is given as

$$q = \begin{cases} p/2, & \text{if } p \text{ is even} \\ (p+1)/2, & \text{if } p \text{ is odd} \end{cases}. \quad (9)$$

The length p is typically chosen based on trial-and-error.

The coefficients \mathbf{a} in (8) are found by minimizing the weighted least-squares cost of the error

$$\epsilon(k) = F_{ij}(e^{-j2\pi k/M}) - H_{ij}(k) = \mathbf{a}^T \mathbf{x}_k - H_{ij}(k), \quad (10)$$

using $z = e^{j2\pi k/M}$ and where

$$\mathbf{x}_k = \left[e^{-j\frac{2\pi k(-q)}{M}}, e^{-j\frac{2\pi k(1-q)}{M}}, \dots, e^{-j\frac{2\pi k(p-q)}{M}} \right]^T,$$

that is, minimizing the standard weighted linear least-squares cost-function [21,22]

$$J(\mathbf{a}) = \sum_{k=0}^{M-1} W(k) \epsilon(k) \epsilon^*(k) = \left\| \mathbf{W}^{1/2} (\mathbf{b} - \mathbf{X}\mathbf{a}) \right\|^2, \quad (11)$$

where $W(k)$ is an error weighting function [21,22],

$$\mathbf{W} = \text{diag} \left([W(0), W(1), \dots, W(M-1)]^T \right),$$

$$\mathbf{b} = \begin{bmatrix} H_{ij}(0) \\ H_{ij}(1) \\ \vdots \\ H_{ij}(M-1) \end{bmatrix}, \text{ and } \mathbf{X} = \begin{bmatrix} \mathbf{x}_0^T \\ \mathbf{x}_1^T \\ \vdots \\ \mathbf{x}_{M-1}^T \end{bmatrix}.$$

where $\mathbf{W} \in \mathbb{R}^{M \times M}$, $\mathbf{b} \in \mathbb{R}^{M \times 1}$, $\mathbf{X} \in \mathbb{R}^{M \times M}$. Note that $H_{ij}(k)$ is the inverse response of the plant from i^{th} input to j^{th} output. The error weighting function can be used to adjust how to weigh the error at different frequencies. Here, a unit weight has been used, i.e. $W(k) = 1$. The MATLAB function `lsqcov` can be used to minimize (11).

If the filter length p is short compared to the measured impulse response, some distortion of the frequency response of (8) can occur. This can be alleviated by using a window function [23]. The impulse response of the windowed FIR filter $\tilde{h}(n)$ created from a non-windowed FIR filter $h(n)$ is given as

$$\tilde{h}(n) = \gamma(n)h(n), \quad (12)$$

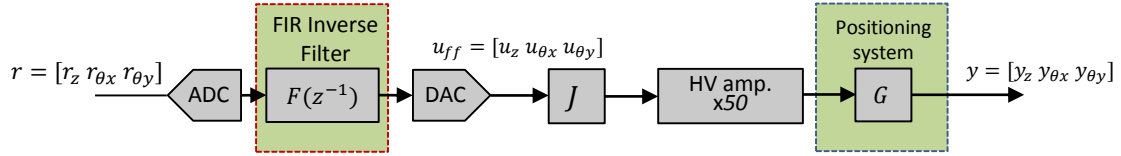


Fig. 5. Block diagram of the inversion-based feedforward control

where $\gamma(n)$ is a window function which is nonzero only for $n = 0, 1, \dots, M-1$. The window function $\gamma(n)$ can be represented in the frequency domain as

$$\Gamma(k) = \sum_{n=0}^{M-1} \gamma(n - M/2) e^{-j2\pi kn/M} \quad (13)$$

$$= \left[\sum_{n=0}^{M-1} \gamma(n) e^{-j2\pi kn/M} \right] e^{-j(2\pi k/M)(M/2)}. \quad (14)$$

Note that the window function is time-shifted to be centred around $n = M/2$ rather than $n = 0$, due to the term $e^{-j(2\pi k/M)(M/2)}$. This phase-shift causes distortion in $\tilde{h}(n)$. To compensate, $h(n)$ also needs to be phase-shifted before windowing. A phase-shift is obtained by a circularly shifting the response by $M/2$ samples, and the phase-shifted impulse response is denoted $\bar{h}(n)$

Applying the window $\gamma(n)$ to the time-shifted impulse response $\bar{f}_{ij}(n)$ of (8), the filter impulse response is

$$\tilde{f}_{ij}(n) = w(n) \bar{f}_{ij}(n), \quad (15)$$

where $\bar{f}_{ij}(n)$ is the phase-shifted impulse response of $f_{ij}(n)$. The FIR filter can then be represented in the z -domain as

$$\tilde{F}_{ij}(z^{-1}) = W(z^{-1}) * \left[z^{-M/2} F_{ij}(z^{-1}) \right]. \quad (16)$$

The filters $F_{ij}(z^{-1})$ are found for each element in the inverse EFTE matrix $\hat{\mathbf{G}}^{-1}(k)$. The resulting filters forms a matrix of FIR filters, denoted $\mathbf{F}(z^{-1})$, that invert the dynamics of the MIMO system.

V. EXPERIMENTAL RESULTS

A. MIMO FIR filter

The frequency responses of the MIMO FIR filter inverse are shown in Fig. 4. As discussed in Sec. IV, the distortion in the frequency response due to the truncation of the non-windowed filter results in a modelling error. However, use of a window function provides a smoothing effect in the frequency response. The responses of the FIR filters with Hann windowing is also shown in Fig. 4.

B. Inversion-based Feedforward Control

Fig. 5 shows a block diagram of an inversion-based feedforward control law. Here, the MIMO FIR filter matrix $\mathbf{F}(z^{-1})$ designed in Sec. IV is used to invert the dynamics of the nanopositioner. In the frequency domain, the feedforward control signal vector \mathbf{U}_{ff} is given by

$$\mathbf{U}_{ff}(z^{-1}) = \mathbf{F}(z^{-1})\mathbf{R}(z^{-1}), \quad (17)$$

TABLE I
TRACKING PERFORMANCE AT 20 HZ. OPEN-LOOP VS. FEEDFORWARD.

	Z-axis		θ_x		θ_y	
	$e_{max}(\%)$	$e_{rms}(\%)$	$e_{max}(\%)$	$e_{rms}(\%)$	$e_{max}(\%)$	$e_{rms}(\%)$
OL	7.8	4.5	7.2	4.9	8.6	5.5
FF	2.8	1.8	3.9	2.8	3.8	3.1

where $\mathbf{r}(t)$ is the input reference vector and $\mathbf{u}_{ff}(t)$ is the vector of feed-forward control signals. The feed-forward control input $\mathbf{u}_{ff}(t)$ is obtained by passing the reference input trajectory $\mathbf{r}(t)$ through the FIR filter inverse of the dynamics of the plant \mathbf{G} . The ideal outcome for the feed-forward control law is to achieve identity (with the inherent delay in the FIR filter), i.e. $\mathbf{G}(z^{-1})\mathbf{F}(z^{-1}) \approx \mathbf{I}_n z^{-M/2}$.

The frequency response of the feed-forward control law from the reference $\mathbf{r}(t)$ to the output $\mathbf{y}(t)$ is shown in Fig. 4. As expected, the response is approximately the identity matrix with unity response over a wide frequency range in diagonal elements and zero response in off-diagonal elements. From the graph, a significant reduction of from 50dB to 100dB in cross-coupling responses can be observed. For instance, the cross-coupling reduction at first resonance frequency for G_{zy} , shown in Fig. 4 is 70dB.

To examine the tracking performance of the feed-forward control law, a 20 Hz triangular wave was applied to each input independently. The performance of the system with and without the FIR filter inverse feed-forward control law is shown in Fig. 6. The tracking performance results compared the case without feed-forward are shown in Table. I.

VI. CONCLUSIONS

In this paper, a method for the design and implementation of a multi-variable model-less inversion-based feed-forward control with FIR inverse filters was presented. The FIR filters were obtained based on the least-squares method using empirical transfer function estimates of the plant. This method overcomes the difficulties associated with non-minimum phase zeros. In addition, it eliminates the need for model-based system identification. The technique was demonstrated on a multi-variable monolithic nanopositioning stage. The experimental results show a significant reduction in the cross-coupling and improved output tracking.

REFERENCES

- [1] A. J. Fleming and K. K. Leang, *Design, modeling and control of nanopositioning systems*. Springer, 2014.

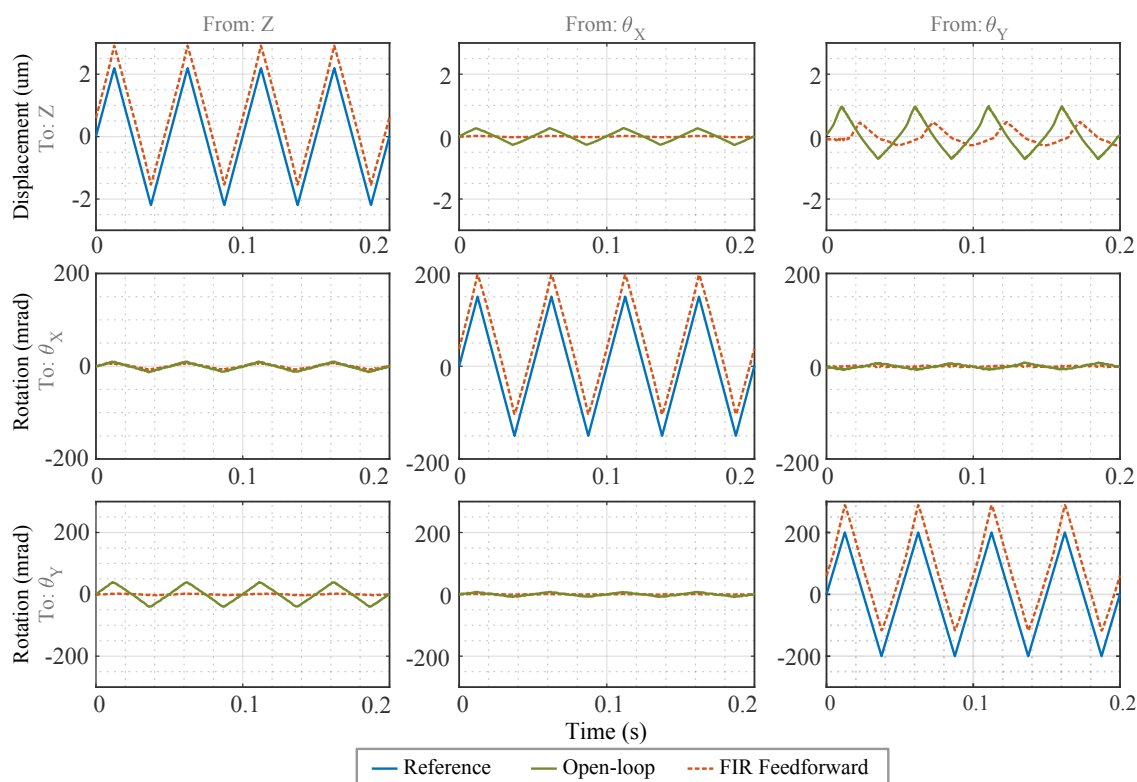


Fig. 6. The tracking and cross-coupling performance of the nanopositioner with feed-forward controller.

- [2] K. K. Leang and S. Devasia, "Feedback-linearized inverse feedforward for creep, hysteresis, and vibration compensation in afm piezoactuators," *IEEE Transactions on Control Systems Technology*, vol. 15, no. 5, pp. 927–935, 2007.
- [3] B. P. Rigney, L. Y. Pao, and D. A. Lawrence, "Nonminimum phase dynamic inversion for settle time applications," *IEEE Transactions on Control Systems Technology*, vol. 17, no. 5, pp. 989–1005, 2009.
- [4] L. Silverman, "Inversion of multivariable linear systems," *IEEE transactions on Automatic Control*, vol. 14, no. 3, pp. 270–276, 1969.
- [5] G. M. Clayton, S. Tien, K. K. Leang, Q. Zou, and S. Devasia, "A review of feedforward control approaches in nanopositioning for high-speed spm," *Journal of Dynamic Systems, Measurement, and Control*, vol. 131, no. 6, p. 061101, 2009.
- [6] A. J. Fleming and Y. K. Yong, "An ultrathin monolithic xy nanopositioning stage constructed from a single sheet of piezoelectric material," *IEEE/ASME Transactions on Mechatronics*, vol. 22, no. 6, pp. 2611–2618, 2017.
- [7] S. I. Moore, M. Omidbeike, A. Fleming, and Y. K. Yong, "A monolithic serial-kinematic nanopositioner with integrated sensors and actuators," in *2018 IEEE/ASME International Conference on Advanced Intelligent Mechatronics (AIM)*, pp. 150–155, IEEE, 2018.
- [8] M. Omidbeike, Y. R. Teo, Y. K. Yong, and A. J. Fleming, "Tracking control of a monolithic piezoelectric nanopositioning stage using an integrated sensor," *IFAC-PapersOnLine*, vol. 50, no. 1, pp. 10913–10917, 2017.
- [9] M. Omidbeike, Y. K. Yong, S. I. Moore, and A. J. Fleming, "A 5-axis monolithic nanopositioning stage constructed from a bimorph piezoelectric sheet," *International Conference on Manipulation, Automation and Robotics at Small Scales (MARSS)*, 2019.
- [10] S. Devasia, "Should model-based inverse inputs be used as feedforward under plant uncertainty?," *IEEE Transactions on Automatic Control*, vol. 47, pp. 1865–1871, Nov. 2002.
- [11] G. B. Giannakis and J. M. Mendel, "Identification of nonminimum phase systems using higher order statistics," *IEEE Transactions on Acoustics, Speech, and Signal Processing*, vol. 37, no. 3, pp. 360–377, 1989.
- [12] M. Tomizuka, "Zero phase error tracking algorithm for digital control," *Journal of Dynamic Systems, Measurement, and Control*, vol. 109, no. 1, pp. 65–68, 1987.
- [13] Q. Zou and S. Devasia, "Preview-based stable-inversion for output tracking of linear systems," *Journal of Dynamic Systems, Measurement, and Control*, vol. 121, no. 4, pp. 625–630, 1999.
- [14] Q. Zou and S. Devasia, "Preview-based optimal inversion for output tracking: Application to scanning tunneling microscopy," *IEEE Transactions on Control Systems Technology*, vol. 12, no. 3, pp. 375–386, 2004.
- [15] D. Croft, D. McAllister, and S. Devasia, "High-speed scanning of piezo-probes for nano-fabrication," *Journal of manufacturing science and engineering*, vol. 120, no. 3, pp. 617–622, 1998.
- [16] Y. R. Teo, A. J. Fleming, A. A. Eielsens, and J. Tommy Gravdahl, "A Simplified Method for Discrete-Time Repetitive Control Using Model-Less Finite Impulse Response Filter Inversion," *Journal of Dynamic Systems, Measurement, and Control*, vol. 138, p. 081002, May 2016.
- [17] A. A. Eielsens, Y. R. Teo, and A. J. Fleming, "Improving Robustness Filter Bandwidth in Repetitive Control by Considering Model Mismatch," *Asian Journal of Control*, vol. 20, pp. 1047–1057, July 2017.
- [18] L. Ljung, *System identification: theory for the user*. Prentice-hall, 1987.
- [19] P. Welch, "The use of fast fourier transform for the estimation of power spectra: a method based on time averaging over short, modified periodograms," *IEEE Transactions on Audio and Electroacoustics*, vol. 15, no. 2, pp. 70–73, 1967.
- [20] L. Rabiner, "Techniques for designing finite-duration impulse-response digital filters," *IEEE Transactions on Communication Technology*, vol. 19, no. 2, pp. 188–195, 1971.
- [21] I. W. Selesnick, M. Lang, and C. S. Burrus, "Constrained Least Square Design of FIR Filters Without Specified Transition Bands," *IEEE Transactions on Signal Processing*, vol. 44, pp. 1879–1892, Aug. 1996.
- [22] J. E. Gentle, *Numerical Linear Algebra for Applications in Statistics*. Springer-Verlag, 1998.
- [23] J. G. Proakis and D. G. Manolakis, *Digital Signal Processing*. Prentice Hall, 1995.